U.S. DEPARTMENT OF THE INTERIOR
U.S. GEOLOGICAL SURVEY

OPEN-FILE REPORT 2007-1006
USGS Afghanistan Project Product No. 110

Introduction

Phyllic and argillic-altered rocks are the result of hydrothermal alteration and are typically associated with porphyry copper and other vein-alteration ore deposits (Lowell and Guilbert, 1970; Cox and Singer, 1986). Alunite and kaolinite are common minerals found in argillic-altered rocks, whereas phyllic-altered rocks typically contain sericite (muscovite).

Phyllic and argillic-altered rocks were mapped in the southern and southeastern parts of Afghanistan using Advanced Spaceborne Thermal Emission and Reflection Radiometer (ASTER) data (Fig. 1). The areas mapped include the volcanic and igneous intrusive rocks of the Chagai Hills in the Helmand and Qandahar provinces, the Argandab igneous intrusive complex in the Zabol and Ghazni provinces and Miocene diorite intrusive rocks in the eastern part of the Zabol province (Chmyriov and Mirzad, 1972). The Chagai Hills and Argandab igneous intrusive complex are part of the Tethyan magmatic arc, which contains extensive copper deposits in Pakistan and Iran (Leaman and Staude, 2002; Mars and Rowan, 2006).

ASTER measures reflected radiation in 3 bands between 0.52 and 0.86 µm (VNIR); in 6 bands from 1.6 to 2.43 µm (SWIR); and emitted radiation in 5 bands in the 8.125 to 11.65 µm wavelength region (TIR) with 15-m, 30-m, and 90-m resolution, respectively (Fujisada, 1995). ASTER also has a back-looking VNIR telescope with 15-m resolution. Thus, stereoscopic VNIR images can be acquired at 15-m resolution. The swath-width is 60 km, but ASTER's pointing capability extends the total cross-track viewing capability to 232 km (Fujisada, 1995). The spectral bands of the ASTER SWIR subsystem were designed to measure reflected solar radiation in one band centered at 1.65 µm, and five bands in the 2.10–2.45 µm region in order to distinguish Al-OH, Fe,Mg-OH, H-O-H, and CO3 absorption features (Rowan and Mars, 2003; Fujisada, 1995). Previous studies document identification of specific minerals, such as alunite, kaolinite, calcite, dolomite, and muscovite, as well as mineral groups, through analysis of ASTER data (Rowan and Mars, 2003; Rowan et al., 2003). Alunite, kaolinite and muscovite have absorption features positioned at 2.165 and 2.2 µm that are defined by ASTER bands 4 (1.65 µm), 5 (2.165 µm), 6 (2.2 µm), and 7 (2.26 µm) (Fig. 2; Mars and Rowan, 2006).

Methods

ASTER level 1-B radiance data (33 scenes) were downloaded from the EROS Data Center and converted to reflectance data using ACORN atmospheric correction software (Acorn, 2003). The 30-m resolution SWIR data were resampled by a factor of 2 to correspond to the VNIR spatial dimensions. The 15-m resolution 6 SWIR and 3 VNIR bands were combined to form 9-band 15 m spatial resolution data sets.

The 33 individual ASTER scenes used in this study were recorded at 4 different viewing angles ranging from nadir to 8.2 degrees off nadir, which causes misregistration of up to 600 m in high relief terrain. Therefore, each 9-band image was geometrically registered to orthorectified Landsat TM data (NASA, 2003). The Landsat mosaic data has a spatial resolution of 28.5 m and spatial accuracy of +/- 50 m. Although this registration procedure corrected for the off-nadir viewing offset, the images were not corrected for terrain displacement. Using a second order polynomial warp registration algorithm and at least 9 ground control points for each ASTER scene produced RMS errors of less than 2.0 (60 m). The mosaic of Landsat 4 and 5 data (band 7) was also used as a base map to illustrate regional ASTER alteration for the study area (Fig. 1). Argillic and phyllic alteration units derived from the ASTER data were converted to vector data and overlain on the Landsat mosaic (Fig. 1).

Correction of ASTER data using Hyperion Hyperspectral Data

Comparisons of ASTER reflectance data to spectra taken in situ from calibration sites in the United States, from laboratory samples, and from calibrated hyperspectral data indicate anomalously low reflectance for ASTER band 5 (Mars and Rowan, 2006). When band 5 is too low the spectra are more similar in shape to argillic minerals such as Alunite (Fig. 2), and the mapping algorithms will overestimate argillic alteration and underestimate phyllic alteration (Mars and Rowan, 2006). Hyperion data were resampled to ASTER bandpasses and used to correct ASTER band 5. Hyperion, a hyperspectral instrument flown on board the EO1 satellite platform, has 196 spectral bands in the 0.45 to 2.4-µm region (Kruse et al., 2003). Although Hyperion coverage is limited to a small subset (10 km orbital swath) of the ASTER data, the Hyperion data can be properly calibrated to reflectance using the additional Hyperion atmospheric bands not available in ASTER data.

Hyperion radiance data were calibrated to reflectance data using ACORN atmospheric removal software. The Hyperion reflectance data were resampled to ASTER VNIR-SWIR bandpasses and georegistered to the orthorectified Landsat TM imagery (NASA, 2003). Average spectra were extracted from areas of overlap for the ASTER and Hyperion scenes. A scalar correction consisting of the ASTER resampled Hyperion band ratio 5/6 divided by the ASTER band ratio 5/6, was applied to all ASTER band 5 data. A total of 4 Hyperion scenes were used to correct the 33 ASTER scenes that covered the study area. An average of the scalar correction value (5.4 percent) was used to correct the ASTER data for the study area.

Logical Operator Algorithms

IDL logical operator algorithms were developed and used to map argillic and phyllic-altered rocks (Fig. 3; ENVI, 2006). For each pixel the logical operator algorithm performs a series of band ratios. Each logical operator determines a true or false value for each ratio by comparing the band ratio to a predetermined range of threshold values. All of the ratios in the algorithm have to be true in order for a value of 1 to be assigned to an output byte image, otherwise a 0 value is produced. Thus, a byte image consisting of zeros and ones is produced with each algorithm. Reflectance hyperspectral data from a calibration site in Cuprite, Nevada, and spectra taken from field samples were resampled to ASTER bandpasses and spectroscopically assessed to determine the range of ratios and band ratio values for constraining the logical operator algorithms (Mars and Rowan, 2006). The logical operator algorithm combines multiple band ratios used to mask dark pixels, green vegetation, and map alteration into a single algorithm which streamlines regional mapping and provides a consistent approach for mapping altered rocks across the entire study area.

Phyllic Band Ratio Logical Operator Algorithm

The first part of the Phyllic Band Ratio Logical Operator (PBRLO) algorithm performs a band 3/2 ratio to mask out green vegetation (Fig. 3A). A spectral analysis of image and library spectra suggests that band 3/2 ratio threshold values of 1.3 and less typically, constitute areas that lack green vegetation. The ratio does not mask out dead vegetation, which has 2.17 and 2.33-µm cellulose absorption features.

The PBRLO algorithm performs a threshold of band 4 to mask out pixels with low reflectance (Fig. 3A). Pixels with low reflectance contain abnormally high band 5 and band 9 values, which may be due to energy leakage from the band 4 detector into adjacent band 5 and band 9 detectors (Iwasaki et al., 2001; Rowan and Mars, 2003). The energy leakage is referred to as "crosstalk" (Iwasaki et al., 2001; Rowan and Mars, 2006). Pixels with low reflectance that are affected by "crosstalk" in this study typically include shadowed areas, and dark, mafic and ultramafic rocks. Abnormally high band 5 and 9 values due to "crosstalk" produce anomalous band 6 and 8 absorption features. Spectral analysis of ASTER image spectra suggests that ASTER band 4 pixels with DN values less than 2600 have inaccurate spectral signatures due to "crosstalk" and, therefore, were excluded using a digital mask.

Spectral analysis of ASTER image spectra and resampled ASTER laboratory spectra showed that band ratios 4/5, 5/6 and 7/6 were needed to map the 2.165 µm and 2.2 µm absorption features, thereby delineating phyllic and argillic alteration (Figs. 2 and 3). Band ratios 4/5 and 5/6 map the 2.165 µm and 2.2 µm absorption features, respectively (Figs. 2 and 3A). Spectral analysis of ASTER spectra indicates that band 5 must be at least 5 percent higher than band 6 in order to map as phyllic alteration, thus, the 5/6 band ratio delineates phyllic from argillic alteration by classing ratio values of higher than or equal to 1.05 as phyllic alteration. ASTER spectra of phyllic-altered rocks also illustrate that band 4 is at least 25 percent higher than band 6, and band 7 is 5 percent higher than band 6. Thus, values in the PBRLO algorithm for band ratios 4/5, and 7/6 must be higher than 1.25, and higher than or equal to 1.05, respectively, to classify a pixel as phyllic alteration (Figs. 2 and 3A).

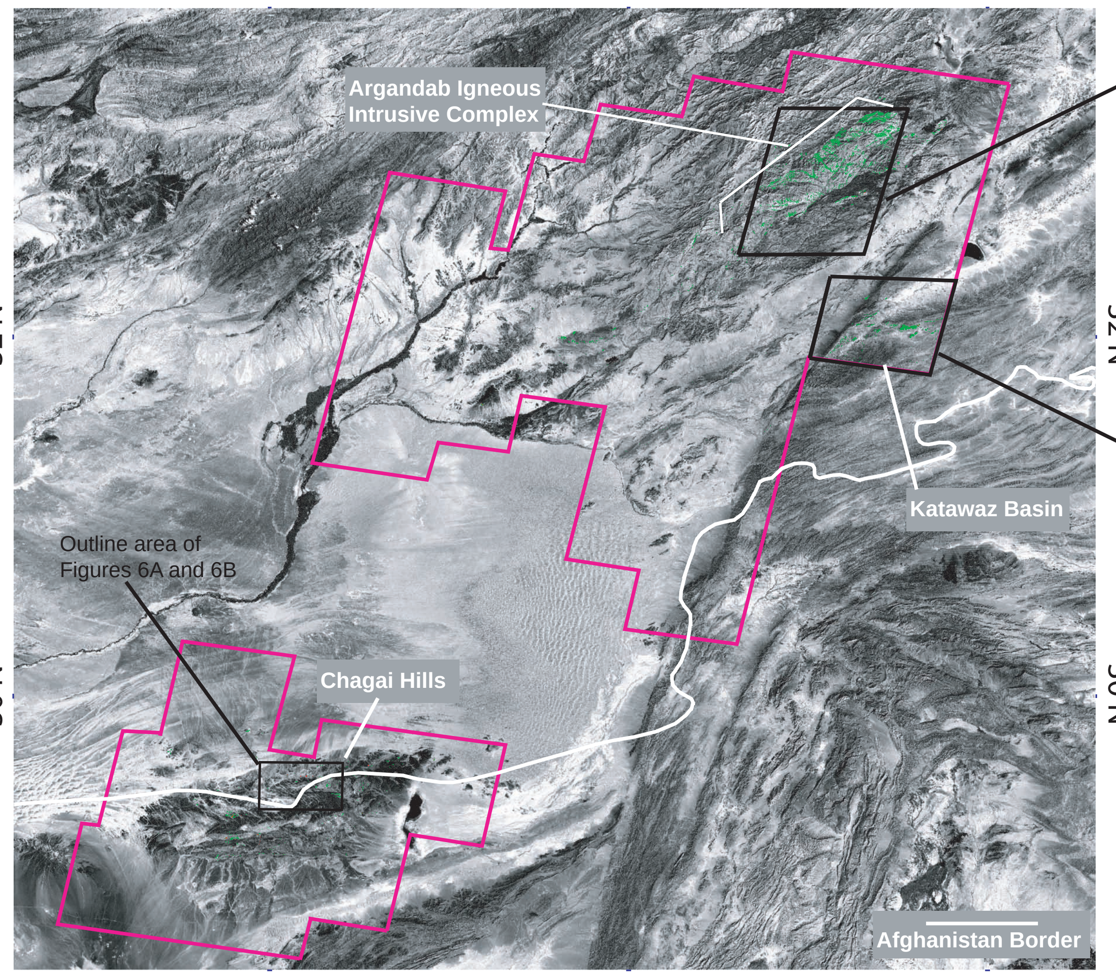

Figure 1. Landsat 4-5 Thematic Mapper mosaic of southeastern Afghanistan with argillic and phyllic alteration units from ASTER data. Alteration units are exaggerated in size.

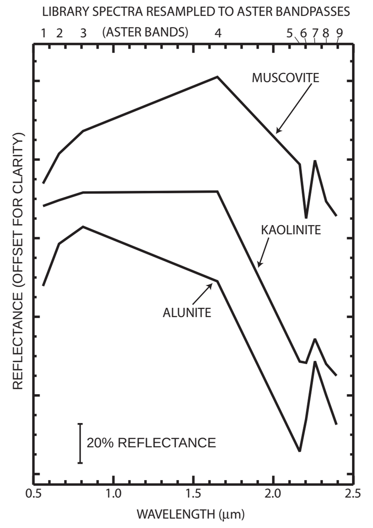

Figure 2. Sample spectra resampled to ASTER bandpasses. Alunite and kaolinite are typically associated with argillic-altered rocks and muscovite is typically associated with phyllic-altered rocks (From Mars and Rowan, 2006).

Inteactive Data Language (IDL)
LOGICAL OPERATORS

(A) Logical operator to map phyllic alteration.

Mask vegetation — Mask dark pixels — Ratio to map 2.200 µm feature associated with phyllic alteration

```
(((float(b3)/b2) le 1.3)and(b4 gt 2600)and((float(b4)/b6) gt 1.25)
and ((float(b5)/b6) gt 1.05) and ((float(b7)/b6) ge 1.05)
```

Ratio to delineate argillic from phyllic alteration — Ratio to map the 2.200 µm feature associated with phyllic alteration

(B) Logical operator to map argillic alteration.

Mask vegetation — Mask dark pixels — Ratio to map 2.165 µm feature associated with argillic alteration

```
(((float(b3)/b2) le 1.3)and(b4 gt 2600)and((float(b4)/b5) gt 1.25)
and((float(b5)/b6) le 1.05)and((float(b7)/b6) ge 1.03))
```

Ratio to delineate argillic from phyllic alteration — Ratio to map the 2.200 µm feature associated with argillic alteration

Explanation of ENVI operators:
float - convert to floating point
le - less than or equal to
gt - greater than
ge - greater than or equal to

Figure 3. Logical operator algorithms used to map phyllic and argillic-altered rocks (ENVI, 2006; Modified from Mars and Rowan, 2006).

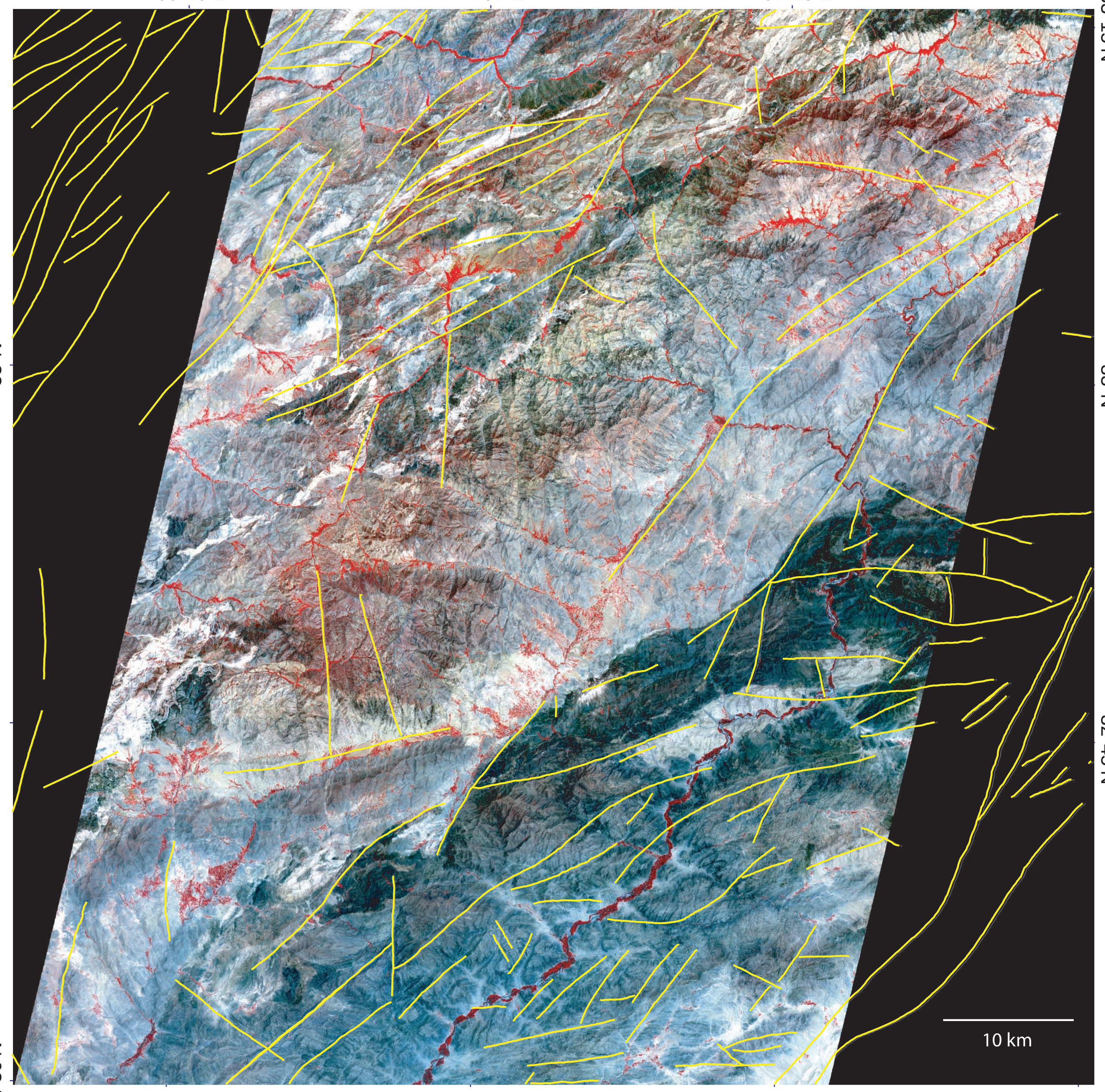

Figure 4A. ASTER false color composite image of the northeast-trending magmatic belt in the Argandab intrusive complex. Vegetation in the image is red. Fault lines in yellow are from the Russian 1:1,000,000 map (Chmyriov and Mirzad, 1972).

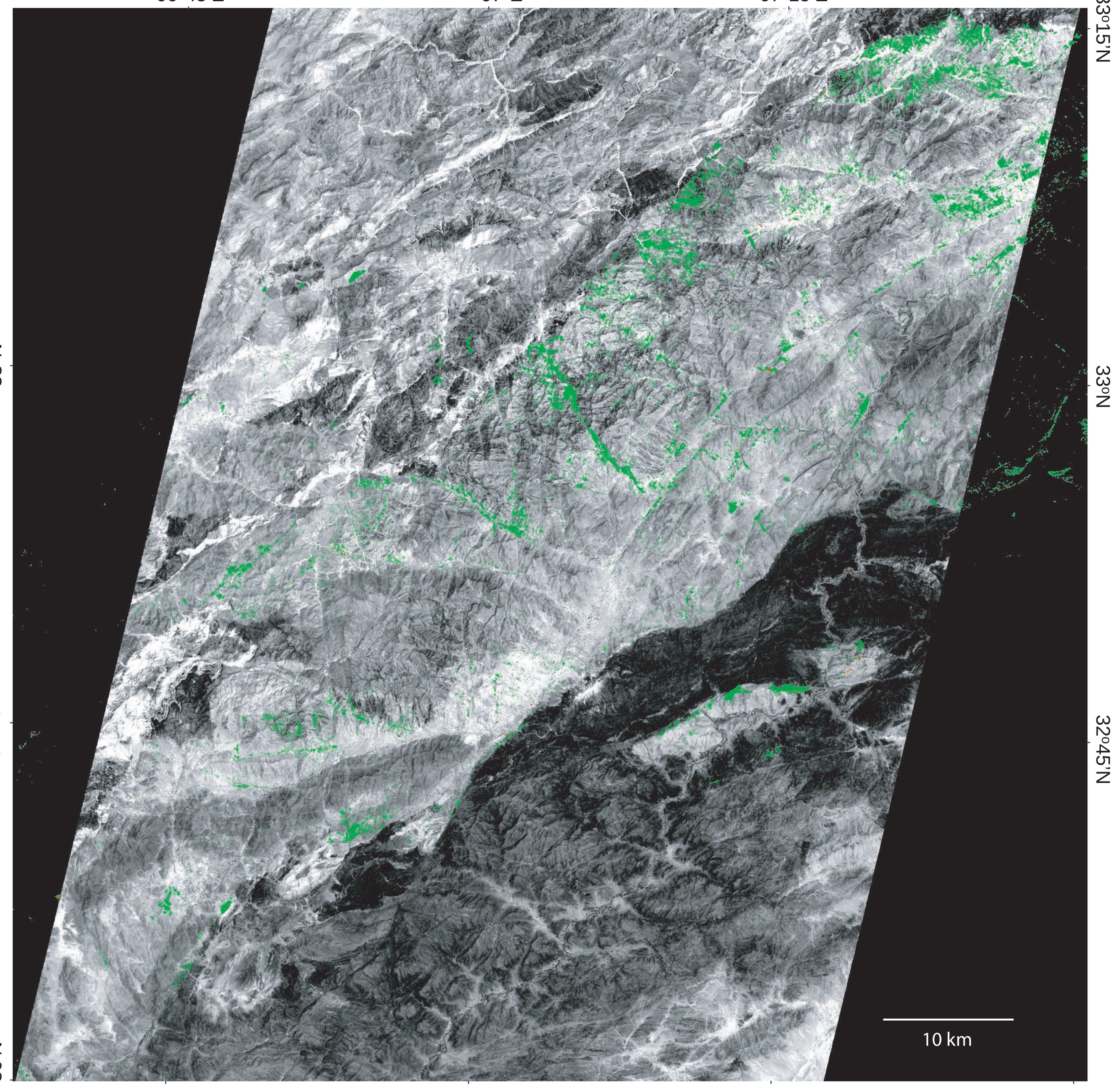

Figure 4B. ASTER image of band 3 and argillic and phyllic alteration of the northeast trending magmatic belt in the Argandab intrusive complex.

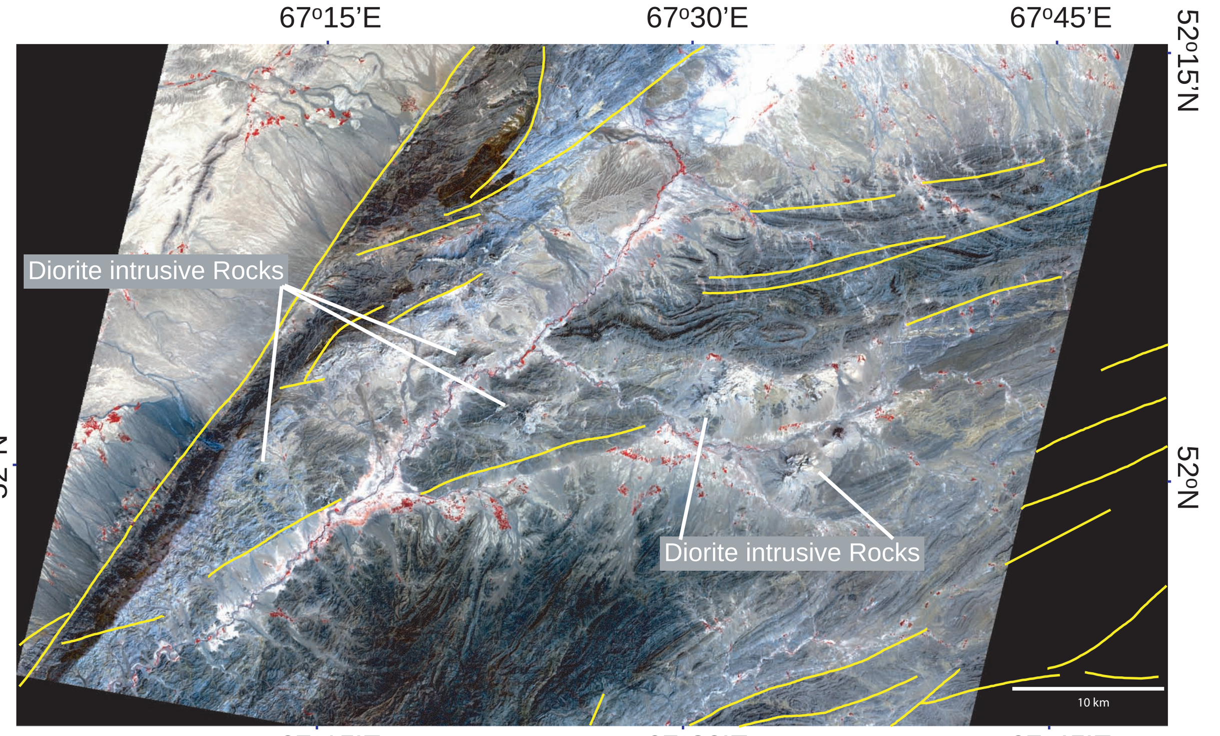

Figure 5A. ASTER false color composite image of Miocene igneous intrusive and lower Tertiary folded sedimentary rocks in the Katawaz basin. Vegetation in the image is red. Fault lines in yellow are from the Russian 1:1,000,000 map (Chmyriov and Mirzad, 1972).

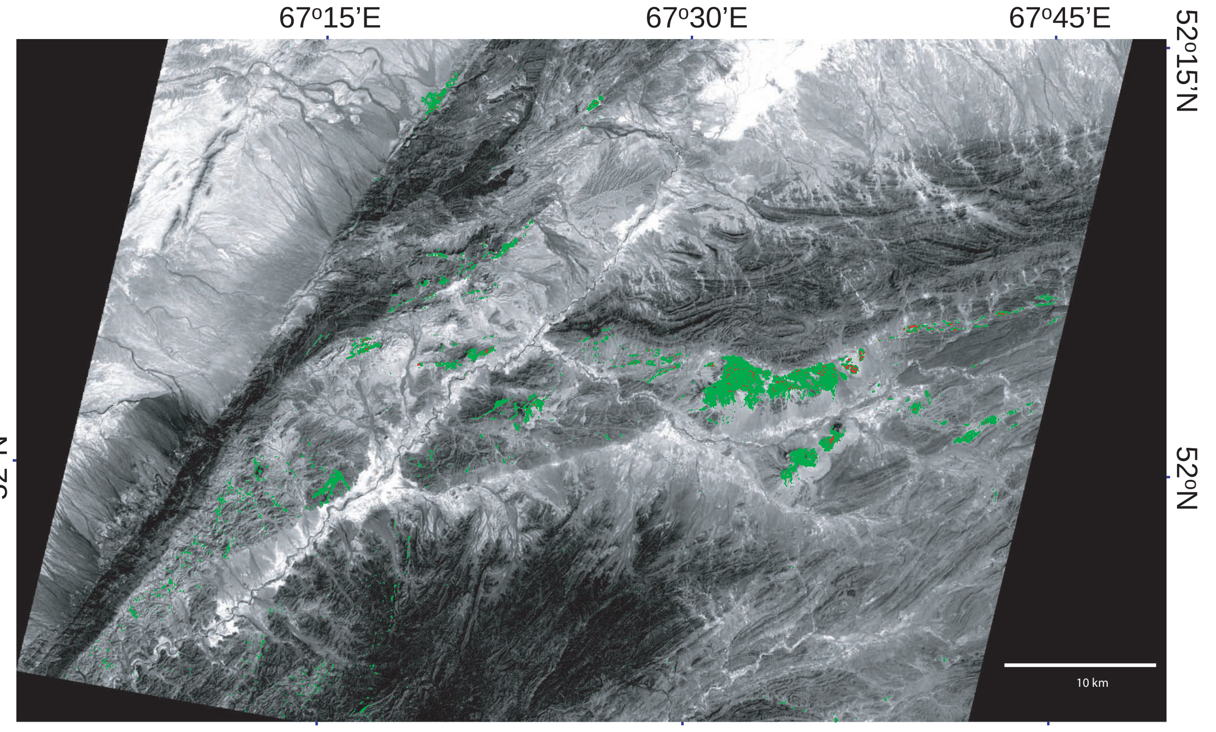

Figure 5B. ASTER image of band 3 and argillic and phyllic alteration of Miocene igneous intrusive and Lower Tertiary folded sedimentary rocks in the Katawaz basin.

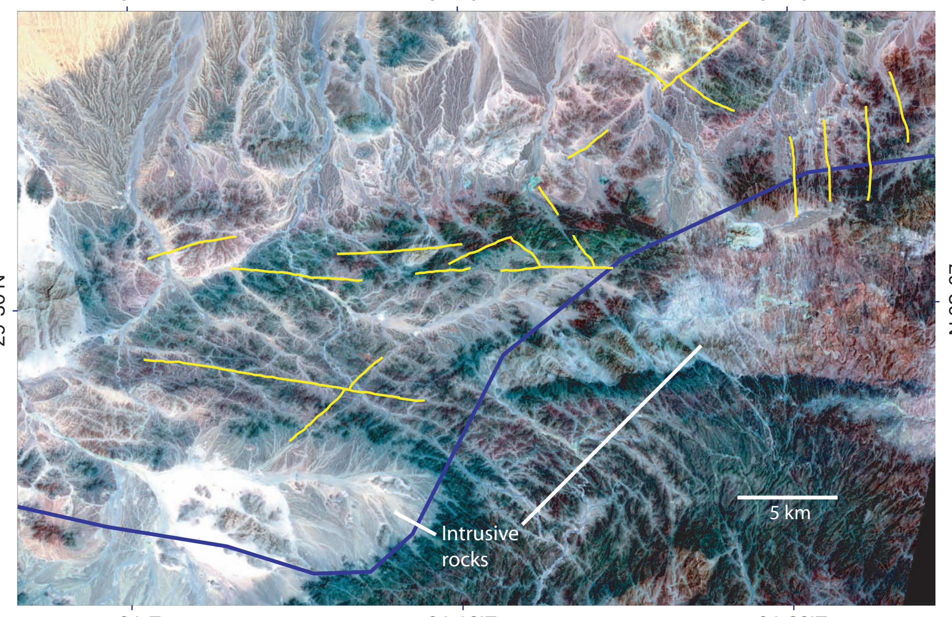

Figure 6A. ASTER false color composite image of Miocene igneous intrusive and volcanic rocks of the Chagai Hills. Fault lines in yellow are from the Russian 1:1,000,000 map (Chmyriov and Mirzad, 1972).

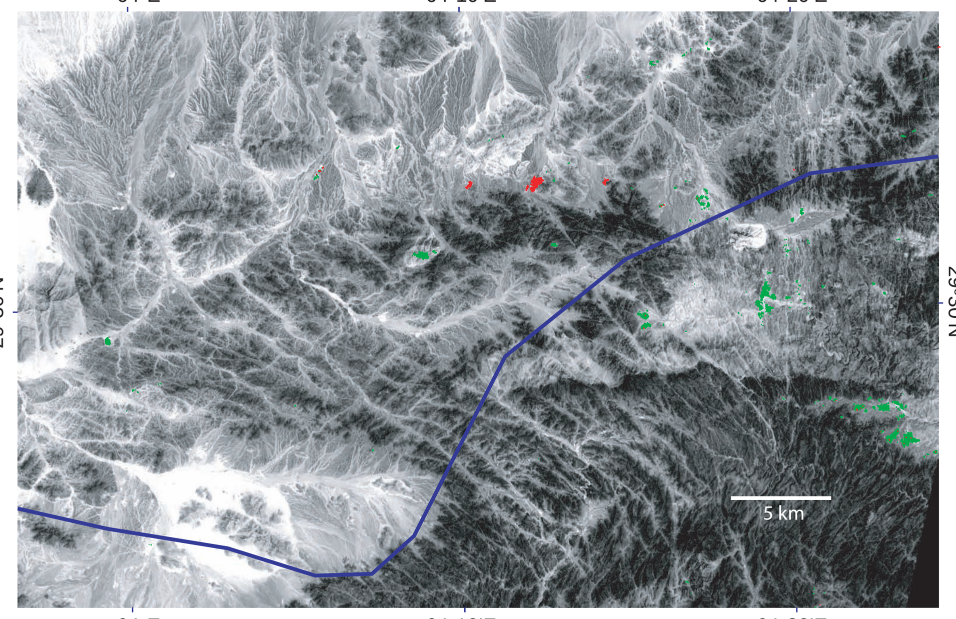

Figure 6B. ASTER image of band 3 and argillic and phyllic alteration of Miocene igneous intrusive and volcanic rocks of the Chagai Hills.

Argillic Band Ratio Logical Operator Algorithm

The Argillic Band Ratio Logical Operator (ABRLO) algorithm is almost identical to the PBRLO algorithm (Fig. 3B). The ABRLO algorithm uses the same methods to mask green vegetation and pixels with low reflectance. An ASTER spectra of argillic-minerals show that band 5 is no more than 5 percent higher than band 6, which is expressed in the ABRLO algorithm as classifying all 5/6 band ratio values less than or equal to 1.05 as argillic alteration (Figs. 2 and 3B). ASTER spectra also indicate that band 5 is at least 25 percent lower than band 4, and band 7 is at least 3 percent greater than band 6. Thus, values in the ABRLO algorithm for band ratios 4/5, and 7/6 must be greater than 1.25, and greater than or equal to 0.03, respectively, in order to classify a pixel as argillic alteration (Figs. 2 and 3B).

Masking detrital clays in sedimentary rocks

Detrital clays in sedimentary rocks can be mistakenly mapped as hydrothermal alteration clay minerals. Many sedimentary rocks such as mudstone, shale, claystone, and litharenite sandstones contain large amounts of detrital clays such as montmorilinite, illite, and kaolinite. In order to mask out detrital clays, an igneous rock mask was produced using the 1:1,000,000-scale Russian geologic map (Chmyriov and Mirzad, 1972). Each map was digitized, georegistered, and polygon vectors were drawn around igneous rock units. The vectors were then converted to a mask, which was applied to the ASTER alteration data, thus, confining alteration mapping to areas underlain by igneous rocks.

Mapping Results

The Argandab intrusive complex contains laterally extensive phyllic altered rocks with very minor amounts argillic altered rocks (Fig. 1). A 15 m resolution false color composite ASTER image (band 3=red, band 2=green, and band 1=blue) of the northern part of the Argandab intrusive complex illustrates a large number of fractures defined by vegetation (red), which correspond to faults taken from the 1:1,000,000 Russian geologic map (Fig. 4A). Hydrothermal alteration patterns are dispersed along fractures and faults and consist of primarily phyllic-altered rocks (Fig. 4B). The dominant patterns of phyllic alteration suggest that vein hydrothermally altered rocks persist at the surface of the Argandab intrusive complex. Known deposits in the area include polymetallic vein copper, zinc, and lead deposits, and copper skarn, and vein gold deposits (United Nations, 1995). Similar associations of deposit types, and alteration patterns and types have been documented along the Tethyan magmatic arc in southwestern Iran (Mars and Rowan, 2006).

A 15 m false color composite ASTER image (band 3=red, band 2=green, and band 1=blue) of the Katawaz basin illustrates a large number of linear features, which correspond to faults taken from the 1:1,000,000 Russian geologic map (Fig. 5A). The rocks in the Katawaz basin are highly folded and intruded by diorite (Fig. 5A). Intrusive rocks contain argillic and phyllic alteration and form elliptical alteration patterns (Fig. 5B). Dominantly phyllic-altered rocks are situated along faults and linear features defined by ASTER data (Fig. 5B). Previous studies suggest that elliptical patterns of phyllic and argillic-altered rocks are commonly associated with porphyry copper deposits and linear patterns of mostly phyllic-altered rocks are associated with hydrothermal vein- altered rocks (Mars and Rowan, 2006). Thus, alteration types and patterns suggest the potential for polymetallic copper, gold, and lead deposits, epithermal gold deposits, and porphyry copper deposits.

An ASTER false color composite image (band 6=red, band 3=green, and band 1=blue) of the Chagai Hills region coupled with Russian fault data indicated extensive faulting and linear features (Fig. 6A). The ASTER false color composite image also delineated igneous intrusive rocks (Fig. 6A). Most alteration is associated with intrusive rocks, however, hydrothermally altered rocks were not as extensive as in the Argandab intrusive complex and the Katawaz basin (Fig. 6B). Whether there are potential porphyry copper or vein style hydrothermal deposits cannot be assessed due to the sparse distribution of mapped phyllic and argillic rocks.

Conclusions

ASTER data and logical operators were successfully used to map phyllic and argillic-altered rocks in the southeastern part of Afghanistan. Hyperion data were used to correct ASTER band 5 and ASTER data were georegistered to orthorectified Landsat TM data. Logical operator algorithms produced argillic and phyllic byte ASTER images that were converted to vector data and overlain on ASTER and Landsat TM images.

Alteration and fault patterns indicated that two areas, the Argandab igneous complex, and the Katawaz basin may contain potential polymetallic vein and porphyry copper deposits. ASTER alteration mapping in the Chagai Hills indicates less extensive phyllic and argillic-altered rocks than mapped in the Argandab igneous complex and the Katawaz basin and patterns of alteration are inconclusive to predict potential deposit types.

References Cited

ACORN, 2003, Atmospheric Correction Now, Version 5.040801, Imspec LLC; http://www.imspec.com/.

Chmyriov, V.M., and Mirzad, S.H., 1972, Geological Map of Afghanistan; Ministry of Mines and Industries of Royal Afghanistan, Department of Geology and Mines [1 sheet, 1,000,000 scale].

ENVI, 2006, ENVI, Version 4.2, ITT; http://www.ittvis.com/envi/index.asp.

Fujisada, H., 1995, Design and performance of ASTER instrument; Proceedings of SPIE, the International Society for Optical Engineering, 2583, p.16–25.

Iwasaki, A., Fujisada, H., Akao, H., Shindou, O., and Akagi, S., 2001, Enhancement of spectral separation performance for ASTER/SWIR, in Proceedings of Infrared Spaceborne Remote Sensing IX, Society of Photo-Optical Instrumentation Engineers, San Diego, California.

Kruse, F. A., Boardman, J. W., and Huntington, J. F., 2003, Comparison of Airborne Hyperspectral Data and EO-1 Hyperion for Mineral Mapping: Transactions on Geoscience and Remote Sensing, IEEE, v. 41, no. 6, p. 1388 - 1400.

Leaman, P., and Staude, J., 2002, Metallogenic evolution of the Western Tethys of Turkey and Iran. Mineral potential of Asia, Metal Mining Agency of Japan, p. 15–18

Mars, J.C., Rowan, L.C., 2006, Regional mapping of phyllic- and argillic-altered rocks in the Zagros magmatic arc, Iran, using Advanced Spaceborne Thermal Emission and Reflection Radiometer (ASTER) data and logical operator algorithms: Geosphere, v. 2, no. 3, p. 161-186.

Rowan, L.C., and Mars, J.C., 2003, Lithologic mapping in the Mountain Pass, California area using Advanced Spaceborne Thermal Emission and Reflection Radiometer (ASTER) data: Remote Sensing of Environment, v. 84, no. 3, p. 350-366.

Rowan, L.C., Hook, S.J., Abrams, M.J., and Mars, J.C., 2003, Mapping hydrothermally altered rocks at Cuprite, Nevada, using the Advanced Spaceborne Thermal Emission and Reflection Radiometer (ASTER), a new satellite-imaging system: Economic Geology, v. 98, no. 5, p. 1019-1027.

NASA, 2003, Applied Sciences Directorate, National Aeronautics and Space Administration; https://zulu.ssc.nasa.gov/mrsid/.

United Nations, 1995, Geology and Mineral Recourses of Afghanistan: Economic and Social Commission for Asia and the Pacific, Atlas of Mineral Resources of the ESCAP Region, New York, v. 11, 85 p.

USGS science for a changing world

USAID FROM THE AMERICAN PEOPLE

ASTER JAPAN/USA

MAPPING PHYLLIC AND ARGILLIC-ALTERED ROCKS IN SOUTHEASTERN AFGHANISTAN USING ADVANCED SPACEBORNE THERMAL EMISSION AND REFLECTION RADIOMETER (ASTER) DATA

By
John C. Mars and Lawrence C. Rowan